Curvature effects on the adsorption of aqueous sodium-dodecyl-sulfate surfactants on carbonaceous substrates: Structural features and counterion dynamics

Naga Rajesh Tummala and Alberto Striolo*

School of Chemical, Biological, and Materials Engineering, The University of Oklahoma, Norman, Oklahoma 73019, USA

(Received 21 April 2009; published 28 August 2009)

The effect of substrate curvature on surfactant self-assembly has been studied using all-atom molecular-dynamics simulations. We studied aqueous sodium-dodecyl-sulfate (SDS) surfactants on graphite, on the outer surface of single walled carbon nanotubes (SWNTs) and within SWNTs. Our results reveal that although the chemical nature of the substrates is constant, the self-assembled structures change significantly as the curvature varies. For example, at large surface density, SDS surfactants yield micellar structures on graphite, layered self-assemblies outside SWNTs, and cylindrical lamellar structures inside SWNTs. Changes in substrate curvature as well as surfactant surface density affect significantly surfactant orientation and, more importantly, headgroup-headgroup distribution, headgroup-counterion packing, and counterion residence time next to the headgroups.

DOI: 10.1103/PhysRevE.80.021408 PACS number(s): 82.70.Dd

I. INTRODUCTION

The self-assembly properties of surfactants are employed in a variety of industrial and research applications [1], including detergents, oil recovery, preparation of mesoporous and hierarchical materials for catalysis, self-healing of surfaces [2], stabilization of carbon nanotubes in aqueous dispersions [3], etc. The process of self-assembly under confinement [4–6] on rough surfaces [2,7–9] and on carbon nanotubes [10–12] has recently attracted scientific attention. For example, surfactants were thought to form cylindrical micellar structures with fully extended tails when adsorbed on carbon nanotubes [3]. On the contrary, it was found that sodium dodecyl sulfate (SDS) surfactants adsorbed on carbon nanotubes yield structures that lack long-range order, as shown by experiments [13], but that show support-specific features and sometimes short-ranged order as suggested by simulations [10,14]. Arai *et al.* [4] showed, employing dissipative particle dynamics simulations, that different polymorphic phases can be obtained when surfactants are confined within nanotubes. The different phases obtained are related to the nature of the nanotube walls and also to the surfactant concentration inside the nanotube. With the aid of lattice Monte Carlo simulations, Zhang *et al.* [5] obtained surfactant morphologies within spherical confinement that had not been observed previously in bulk systems. The results just summarized clearly show that curvature plays a major role in determining the morphology of adsorbed surfactant aggregates. This stimulated our interest in conducting systematic molecular-dynamic simulations to understand the effect of curvature on the morphology of self-assembled surfactant structures.

In this paper, we compare the morphology of the self-assembled aqueous aggregates of the anionic SDS surfactant when adsorbed on one (6,6) single walled carbon nanotube (SWNT), within one (40,40) SWNT, and on graphite. We found that surface curvature strongly affects the aggregate morphology. As the surfactant concentration increases, we observe a planar-to-hemicylindrical transition on flat surfaces, whereas on nanotubes we find a single-to-multilayer transition. Surfactants adsorbed inside nanotubes yield a completely different morphology; they form cylindrical lamellar structures even at low surface coverages. As expected because of hydrophobic considerations, we found that for SDS surfactants adsorbed on the outer surface of nanotubes, as well as on graphite, the hydrophobic tails lie on the support surface. However, when the SDS surfactants adsorb inside a carbon nanotube, the tails are never adsorbed completely on to the surface. Inside (40,40) SWNTs, the surfactant tails extend into the aqueous solvent, and this phenomenon becomes more pronounced as the SDS density increases. We also found that the residence time of sodium counterions near the surfactant headgroups is inversely proportional to the substrate curvature.

II. COMPUTATIONAL DETAILS

Aqueous SDS surfactants were simulated at contact with (6,6) SWNT, (40,40) SWNT, and graphite surfaces. The chiral vector (n,m) represents the dimension, type (arm chair vs zigzag), as well as chirality of SWNTs. The diameters of (6,6) and (40,40) SWNTs calculated as the distance between the center of carbon atoms comprising the nanotubes are $\sim$0.807 and $\sim$5.42 nm, respectively. Within these substrates, the carbon atoms treated as Lennard-Jones spheres were maintained fixed throughout the course of the simulations. Water molecules were modeled using the simple point charge extended (SPC/E) model [15]. The details of the force field employed are described in Ref. [16]. The simulation package GROMACS [17–19] was employed to integrate the equations of motion. In our simulations, the number of particles (N), the simulation box volume (V), and the temperature (T) were maintained constant. Orthorhombic simulation boxes were considered in all cases and periodic boundary conditions were implemented in the three dimensions. Graphite is always parallel to the x-y plane in the simulation

*Author to whom correspondence should be addressed. FAX: 405 325 5813; astriolo@ou.edu

TABLE I. Simulation box size, total number of SDS and water molecules, and surfactant coverage for each of the systems simulated.

Substrate	Label	Box size (nm^3)	No. of SDS	No. of water molecules	Surfactant coverage (nm^2/headgroup)
(6,6) SWNT	66-I	$7.0\times7.0\times6.1487$	16	9900	1.8
(6,6) SWNT	66-II	$7.0\times7.0\times6.1487$	36	9000	0.8
(6,6) SWNT	66-III	$7.0\times7.0\times6.1487$	64	8800	0.45
Graphite	GRA-I	$9.102\times4.26\times20.0$	38	7600	1.02
Graphite	GRA-II	$6.15\times3.124\times25.34$	32	5050	0.60
Graphite	GRA-III	$3.936\times2.556\times25.0$	25	3000	0.40
(40,40) SWNT[a]	I-4040	$10.8\times10.8\times6.1487$	89	3304	1.03
(40,40) SWNT[a]	II-4040	$10.8\times10.8\times6.1487$	108	3000	0.85
(40,40) SWNT[a]	III-4040	$10.8\times10.8\times6.1487$	192	1680	0.48

[a]SDS and water molecules are inside one (40,40) carbon nanotube.

box, and the carbon nanotube axis is always parallel to the z direction. In all simulations, the time step was 2 fs. The Nose-Hoover thermostat [20] with leapfrog algorithm [20] was implemented with a relaxation-time constant of 100 fs. All simulations were conducted at 300 K. Dispersive attractions and repulsive interactions were treated as Lennard-Jones potentials with an inner cutoff of 0.8 nm and an outer cutoff of 1.0 nm. Long-range electrostatic interactions were treated using the particle mesh Ewald [21] method. Bond lengths and bond angles in water were maintained fixed using the SETTLE algorithm [22]. All the simulations were conducted for 50 ns. Only the last 10 ns were used for data analysis. Other simulation details, including the number of molecules simulated and the size of the simulation boxes, are reported in Table I. The labels given in Table I are used throughout the text to refer to the respective simulated systems. The number of simulated molecules was chosen so that the density of the system corresponds to that in the bulk. For the simulation involving (40,40) SWNTs, surfactant and water molecules were present only inside the SWNT. Because GROMACS 3.3.1 does not allow us to simulate systems periodic in only one dimension, periodic boundary conditions were implemented in the three dimensions, but the SWNT was separated from its periodic replicas along the x and y directions by a vacuum of thickness 5.4 nm. Increasing the vacuum thickness to 16.2 nm changes the total system energy by less than 0.5%. For the system containing (6,6) SWNTs, one SWNT was placed at the center of the simulation box surrounded by surfactants and water molecules. In the case of graphite, either two opposing surfaces separated by more than 10.0 nm or one free standing surface covered by a thin aqueous film was considered. Our previous work [16] demonstrates that the results are independent of the configuration chosen. In most cases, SDS surfactants are separated from the periodic replica of the simulated system by at least 6.2 nm. Our previous work [16] guarantees that reliable results are obtained when such distance is larger than 4.5 nm. To further assess the reliability of our results, additional simulations were conducted within the *NPT* ensemble ($P=1$ bar) for SDS surfactants on (6,6) SWTNs (system 66-III in Table I), and the results did not show appreciable differences compared to those shown herein (details can be found in Appendix B). Note that in the implemented *NPT* ensemble, the pressure was maintained constant by allowing the system volume to fluctuate along the x and y directions, while the z dimension was maintained constant because of the presence of the rigid SWNT. Other details of the simulation setup are described in our previous publications [14,16]. It is worth pointing out that the surface area available per each SDS headgroup shown in Table I was calculated by considering excluded volume effects, i.e., the SWNT diameter was increased/decreased by 0.3 nm to account for the size of carbon atoms. The value of 0.3 nm was chosen based on the results for density profiles—showed later—which indicate that no molecule can be found at distances less than $\sim$0.3 nm from the center of the carbon atoms.

III. RESULTS AND DISCUSSION

A. Morphology of self-assembled aggregates

Ionic surfactants with 12 or more methyl groups are known to form hemicylinders at the water-graphite interface at high surface densities [23–25]. At low surface densities, they form monolayers, the orientation of which depends on the length of the tailgroup [26,27]. We found that SDS molecules on graphite orient preferentially along the symmetry α axes when the surface area available for each surfactant headgroup is ~1 nm^2. We compare here the aggregate morphology of SDS adsorbed on (6,6) SWNTs, graphite, and inside (40,40) SWNTs. To visualize the difference in surface aggregate morphology, in Fig. 1 we show representative simulation snapshots of the 66-I, GRA-I, and I-4040 systems (see Table I for details). The surface area available to each surfactant is 1.8 nm^2 in the case of surfactants on (6,6) SWNTs and ~1 nm^2 in the other two cases. For SDS on the (6,6) SWNT, the surfactants form a ringlike structure, similar to the one that has been observed from simulations of zwitterionic lysophosphatidylcholine on SWNTs [10]. Experimental TEM analysis, although performed on dry samples, corroborates the ringlike morphology for surfactants on narrow SWNTs [12]. From our simulations, we notice that al-

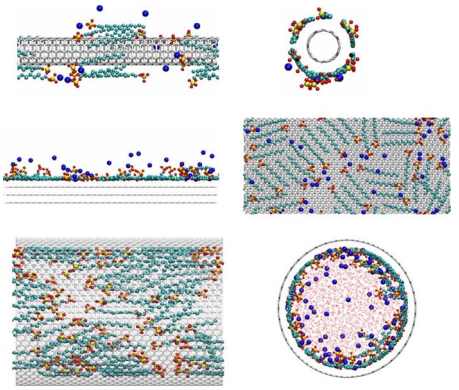

FIG. 1. (Color online) Side and front views of representative simulation snapshots for SDS surfactants on (6,6) SWNTs (system 66-I, top), on graphite (system GRA-I, middle), and inside (40,40) SWNTs (system I-4040, bottom). Methyl groups, oxygen, sulfur, and sodium atoms are represented as cyan, red, yellow, and blue spheres, respectively. Carbon atoms in graphite and carbon nanotubes are shown as bonded carbon atoms. Water, when shown, is represented according to the wireframe representation. All images are generated using the software VMD [28].

though most SDS molecules adsorb completely flat on the SWNT surface, some of the headgroups, and the methyl group closest to the headgroup, project into the aqueous phase. The fraction of SDS headgroups that protrude away from the hydrophobic surface is larger when SDS is adsorbed on graphite (GRA-I) and inside (40,40) SWNT. As discussed earlier [27], SDS at low surface densities on graphite yields a monolayer with a preferential orientation. In the right middle panel of Fig. 1, we observe that SDS surfactants are uniformly distributed on the graphite surface and that the surfactant molecules are oriented parallel, antiparallel, or at $\sim 60^\circ$ to each other. When SDS surfactants are simulated inside (40,40) SWNTs, they yield a cylindrical monolayer-like structure with the SDS molecules oriented parallel to the axis of the nanotube. Within this structure, the headgroups of several SDS molecules protrude toward the aqueous phase at the center of the (40,40) SWNT.

In Fig. 2 we show representative simulation snapshots for the surface aggregates observed when the surface coverage of SDS surfactant exceeds that required to form one monolayer. On graphite (system GRA-II in Table I, middle panels of Fig. 2), although the surfactant tails remain to some extent parallel to the α-axes, the adsorbed SDS surfactants yield multiple layers. The orientation of the SDS molecules adjacent to the graphite substrate not only depends on the SDS-graphite but also on SDS-SDS interactions.

SDS molecules on (6,6) SWNTs (system 66-II in Table I, top panels of Fig. 2) aggregate without completely covering the surface. This suggests that SDS-SDS interactions dominate SDS-SWNT interactions.

Aqueous SDS surfactants within (40,40) SWNTs (system II-4040 in Table I, bottom panels of Fig. 2), at surface density of 0.85 nm^2 per headgroup, yield a threadlike micellar structure. We found that the probability for the SDS headgroups to protrude away from the surface increases as the SDS surface density increases within (40,40) SWNTs (results not shown for brevity).

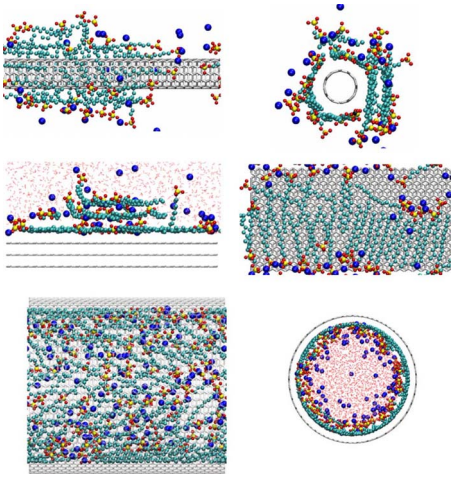

FIG. 2. (Color online) Representative simulation snapshots for SDS surfactants adsorbed on (6,6) SWNTs (system 66-II, top), on graphite (system GRA-II, middle), and inside (40,40) SWNTs (system II-4040, bottom). The color code is the same as in Fig. 1.

At the highest surface density considered here (systems 66-III, GRA-III, and III-4040 in Table I), SDS molecules form hemicylinders at the graphite-water interface, in agreement with experiments [24] and simulations [16,29] (see middle panels in Fig. 3).

As shown in Fig. 3, we find that on (6,6) SWNTs, adsorbed SDS yield multilayer micellar structures. The morphology predicted from our simulations agrees with the experimental neutron-scattering results of Yurekli *et al.* [13], as discussed at length elsewhere [14].

Inside (40,40) SWNTs (system III-4040 in Table I), the aggregate morphology is reminiscent of reverse micelles. It appears that the hydrophobic nanotube provides the support for the hydrophobic surfactant tails. The aggregate resembles a cylindrical micelle, although the aggregate structure is not completely symmetric with respect to x and y axes, as observed in the bottom panels of Fig. 3, because the SDS tail-

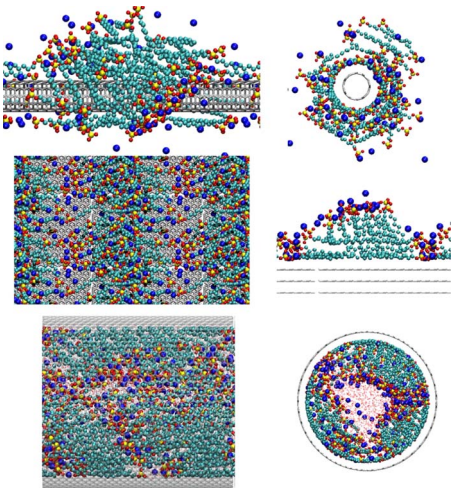

FIG. 3. (Color online) Representative simulation snapshots for SDS surfactants adsorbed on (6,6) SWNTs (system 66-III, top), on graphite (system GRA-III, middle), and inside (40,40) SWNTs (system III-4040, bottom). The color code is described in Fig. 1.

groups extend to different extents toward the center of the nanotube. The aggregate structure just discussed agrees with that reported by Arai *et al.* [4], who simulated coarse-grained surfactants inside hydrophobic nanotubes. Those authors predicted that the threadlike micellar phase gives way to bilayer micelles as the surfactant volume fraction within the nanotube increases. In addition, our all-atom simulations allow us to assess the structure of confined counterions and water molecules. We observe that water molecules yield a helical pattern between the surfactant headgroups along the length of the nanotube. The water molecules are strongly correlated with both SDS headgroups and sodium counterions, yielding a tightly packed structure due to electrostatic effects. We speculate that this cooperative effect involving headgroups, counterions, and water molecules becomes more significant as both the degree of confinement and the surfactant density increase. Strong water-water association is not surprising, as it is well known that water-water hydrogen bonds become stronger under hydrophobic confinement [30,31]. Further, our results show that under confinement water is strongly attracted to charged species (i.e., the SDS headgroups) yielding both dense water-rich region and water-depleted regions, in agreement with the theoretical suggestions of Rasaiah *et al.* [31]. More details about the morphology of SDS aggregates on the three substrates are discussed in Appendix A.

To rationalize the results we invoke geometric arguments. The packing factor of Israelachvili for SDS is less than 0.33 and, hence, SDSs form spherical micelles in aqueous bulk solutions at the critical micelle concentration [1]. In the presence of high concentrations of electrolytes, because of electrostatic shielding between headgroups, SDSs yield long cylindrical micelles [32]. On planar graphite substrates, strong tail-substrate interactions promote a preferentially oriented monolayer, which becomes a hemicylinder as the SDS surface density increases because of the strong tailgroup-tailgroup interactions. Curved substrates impair tail-substrate and tail-tail interactions considerably. For example, in the case of SDS within (40,40) SWNTs, should the surfactants extend radially toward the nanotube center with the tailgroups fixed at the nanotube surface, the distance between different surfactants would decrease as we move from the nanotube surface toward the center of the nanotube. Therefore, confinement effects reduce the headgroup-headgroup distance. Equilibration of the consequent headgroup-headgroup electrostatic repulsion can only be achieved by tight packing of headgroups with counterions and water molecules. In a different scenario, should SDS on (6,6) SWNTs extend radially with their tails on the SWNT surface, the surfactant-surfactant distance would increase moving away from the nanotube. This would increase the hydrophobic surface area exposed to water, clearly an unfavorable phenomenon. Consequently, SDS surfactants on (6,6) SWNTs form randomly aggregated structures with multiple layers in which tail-tail contacts are maximized and tail-water contacts are minimized. These effects can be ascribed to changes in tailgroups effective volume and headgroups effective cross-sectional area due exclusively to the substrate curvature.

B. Radial distribution functions

To understand the effect of curvature and surface coverage on headgroup-headgroup and headgroup-counterion

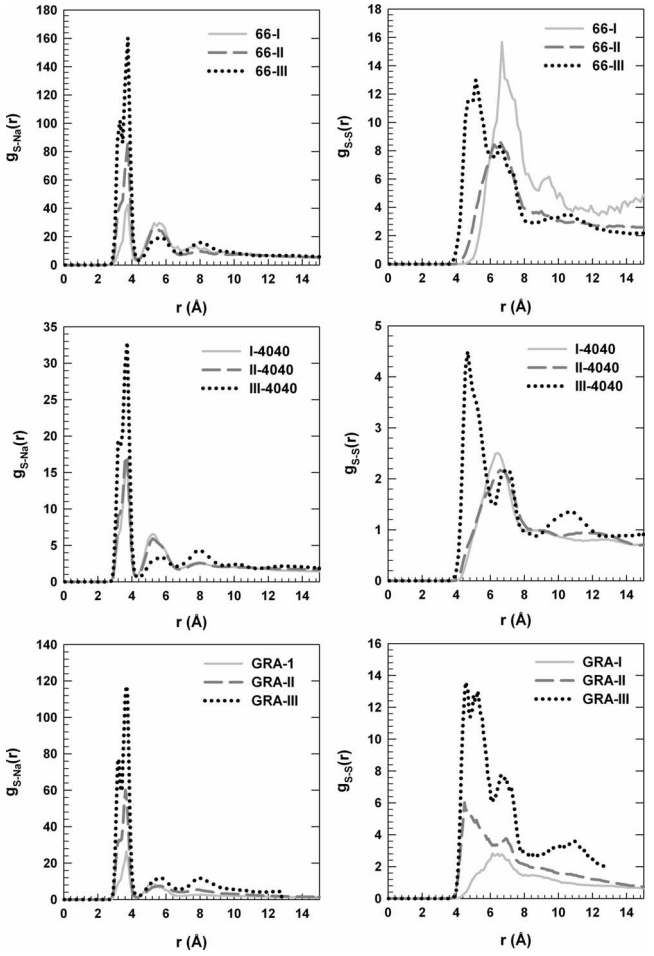

FIG. 4. Sulfur-sodium (left panels) and sulfur-sulfur (right panels) radial distribution functions. Top panels report results for SDS on (6,6) SWNTs, middle panels for SDS inside (40,40) SWNTs, and bottom panels for SDS on graphite. Results are shown at increasing surface coverage. Simulation details can be found in Table I.

structuring, we calculated sulfur-sodium and sulfur-sulfur radial distribution functions (RDFs). Sulfur-sodium and sulfur-sulfur RDFs are representative of surfactant head-counterion and surfactant head-surfactant head RDFs. To account for curvature effects in the calculation of RDFs, we employed an algorithm similar to that proposed by Striolo *et al.* [33]; i.e., we normalize the distribution functions calculated in our simulations with the distribution functions obtained with molecular-dynamic simulations involving ideal-gas particles of density equal to that of SDS surfactants in the corresponding simulations. The results are shown in Fig. 4. The sulfur-sodium RDFs for surfactants on (6,6) SWNTs (top left panel) and on graphite surface (bottom left panel) are similar in terms of peak positions, but the peak intensities differ substantially. Both the RDFs at low surface coverage (compare 66-I and GRA-I systems) have an intense peak at ~4 Å and a small shoulder at 3.2 Å. The intensity of the shoulder at 3.2 Å increases as the surface coverage increases until a clearly discernable peak forms in the case of GRA-III and 66-III systems. The sulfur-sodium RDFs obtained inside (40,40) SWNTs (center left panel of Fig. 4) exhibit different behavior. Instead of the peak observed at 3.2 Å for sulfur-

sodium RDFs on (6,6) SWNTs and graphite at high surface densities, a shoulder appears within (40,40) SWNTs. The intensity of the peaks at ~4.0 Å and ~5.5 Å for low and intermediate surface densities (systems I-4040 and II-4040) are almost identical, although the intensity of the peak at ~4.0 Å and that of the shoulder at ~3.2 Å increase at the highest surface density studied (system III-4040). These data suggest that the high surfactant concentration coupled with the small amount of solvent available promotes packing between the headgroups and sodium counterions within (40,40) SWNTs.

Results from the sulfur-sulfur RDFs are more intriguing and clearly highlight the effects of the curvature on the local arrangement of the surfactant headgroups with respect to each other. On graphite, at low surface coverage the headgroup-headgroup attractions are minimal, as indicated by the first weak peak at ~6.5 Å (bottom right panel of Fig. 4). As the surfactant surface density increases, the counterion-condensation phenomenon described in our previous work [16] becomes more evident, as suggested by the S-Na RDFs shown in bottom left panel of Fig. 4. As a consequence, the headgroups associate more strongly, leading to more intense first peaks in sulfur-sulfur RDFs that are now located at ~4.0 nm (bottom right panel). This systematic increase in headgroup-headgroup packing is only observed on the flat graphite surface but not on the other substrates considered.

On (6,6) SWNTs, as discussed in previous sections, the surfactants form "rings" at low surface density (66-I) around the nanotubes. Consequently, the headgroups are spaced far apart from each other (see peak at ~7 Å in the top right panel of Fig. 4). When the surface density increases (system 66-II), the surfactant headgroups pack closer and the RDF intensity at ~7 Å decreases; the first RDF peak position shifts to shorter distances.

The sulfur-sulfur RDFs computed inside (40,40) SWNTs show very atypical behavior. The peaks in these RDFs show no systematic increases or position shifts as the surface density increases, suggesting that the local packing for SDS inside (40,40) SWNTs does not depend on surface coverage until a critical coverage is reached. At high surfactant concentration, the RDFs on different substrates show strong headgroup-headgroup packing.

C. Density profiles

The density profiles of SDS headgroups, SDS tailgroups, and sodium ions away from the carbon-based substrates are shown in Fig. 5. The center of mass of the sulfate group is used to calculate the density profile for surfactant headgroups. The headgroup density profile for I-4040 and GRA-I systems (top left panel of Fig. 5) indicate that it is equally probable to find the headgroups at 0.35 and 0.55 nm away from the substrate surface. The peak at 0.55 nm and the shoulder at 0.75 nm show that a few headgroups project away from the carbonaceous substrate toward the aqueous phase. The density profiles of the tailgroups in 66-I, GRA-I, and I-4040 display a strong first peak at 0.35 nm, as shown in the middle left panel of Fig. 5, indicating that most of the

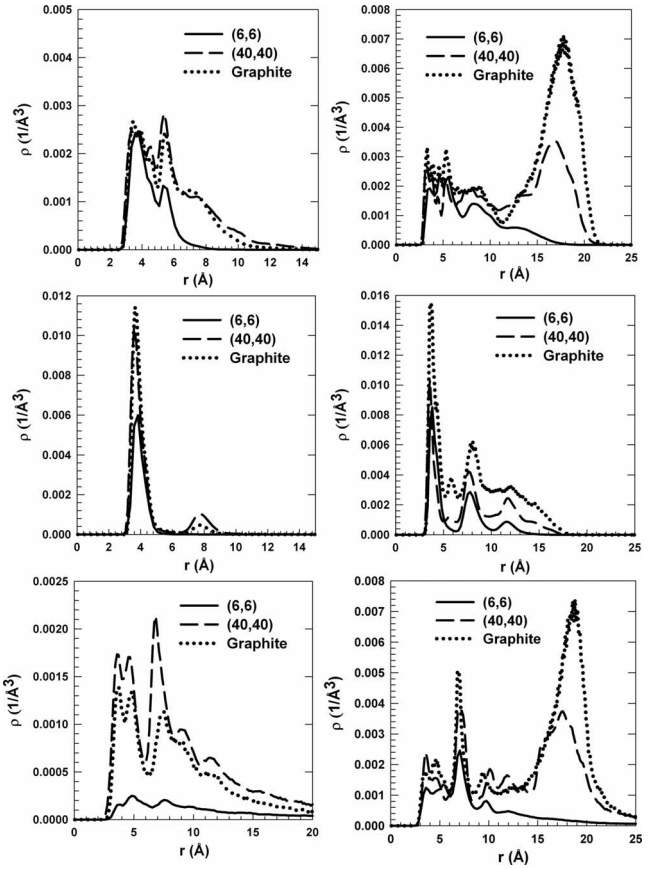

FIG. 5. Headgroup (top), tailgroup (middle), and counterion (bottom) density profiles as a function of distance from the surface for the systems at low SDS surface density (systems 66-I, GRA-I, and I-4040, left panels) and at high SDS surface density (systems 66-III, GRA-III, and III-4040, right panels). See Table I for simulation details.

tailgroups remain at contact with the substrate. Only a small fraction of tailgroups are not completely adsorbed as can be observed from the peak at 0.8 nm.

In the density profile of counterions shown in the bottom left panel of Fig. 5, we observe that on (6,6) SWNTs (system 66-I) the counterions do not accumulate at the SDS-SWNT interface as much as they do on the other substrates considered. SDS adsorption on electrically neutral hydrophobic surfaces generates an electric charge density near the surface that promotes accumulation of the counterions. It is worthwhile to point out that at low surface density, for SDS adsorbed on graphite and within (40,40) SWNTs counterion density peaks are half the headgroup density peaks; whereas on (6,6) nanotubes, the counterion density peak intensity is significantly less than half the peak intensity of the headgroup density profile. Surface curvature affects the surfactant aggregate morphology and, hence, also affects the density distribution of the counterions. At low surface coverage, when the adsorbed surfactants form a single monolayer, it is possible to compare the results of counterion distribution simulated to those predicted by theoretical models such as Manning's condensation theory [34,35], which invokes the Debye-Huckel approximation [36]. The Manning's condensation theory predicts that a spherical surface provides little

or no counterion condensation, cylindrical surfaces tend to accumulate few counterions above a critical surface charge density, and flat surfaces accumulate the highest concentration of counterions [37]. The condensation theory assumes that the counterion density far away from the surface is negligible; thus, direct comparison of the counterion distribution inside the (40,40) SWNT even at low surface coverage is not possible. Cumulative density profiles obtained from Fig. 5 (not shown for brevity) show that counterions in the GRA-I system do not completely accumulate on graphite, even when covered by SDS. Instead, we find that a few sodium ions remain in the bulk liquid and near the vacuum-water interface (in qualitative agreement with Ref. [38]). Counterion-condensation effects are more pronounced inside the SWNTs, due to confinement, than on graphite or on (6,6) SWNTs. The multiple peaks for counterions observed even at low surface density are consequence of excluded volume effects and of ion-ion correlations.

At high surface density, the density profiles for headgroups (top right panel of Fig. 5) and tailgroups (middle right panel of Fig. 5) are consistent with the formation of multilayer structures on (6,6) SWNTs, hemicylindrical micelles on graphite, and reverse micelles within (40,40) SWNTs. In the counterion density profiles for systems 66-III, GRA-III, and III-4040 (bottom right panel of Fig. 5), we observe that the density peaks are positioned at the same distance from the surface as observed for the density profiles of the surfactant headgroups, indicating close packing of headgroups and counterions. In particular, at ~ 1.7 nm from each substrate the counterion density is almost equal to the headgroup density. These data, which support the conclusion that the morphology of surfactant aggregates strongly depends on the substrate curvature, cannot be easily compared to predictions from the Manning's condensation theory because the identification of a smooth interface is not unequivocal.

D. Surfactant headgroup-counterion residence correlation functions

Because the results discussed above suggest that the counterions are strongly correlated with the surfactant headgroups, it is of interest to quantify how long each counterion resides in contact with any given surfactant headgroup. The corresponding residence autocorrelation function is calculated herein as

$$C(t) = \left\langle \frac{\sum_{i=1}^{N} O_i(t) O_i(0)}{\sum_{i=1}^{N} O_i(0) O_i(0)} \right\rangle. \quad (1)$$

In Eq. (1) angular brackets designate ensemble averages and the term $O_i(t)$ discriminates whether a sodium ion is or is not in the vicinity of one SDS headgroup (i.e., within a distance of 4.38 Å, which corresponds to the first minimum in the S-Na radial distribution function) at time t. $O_i(t)$ equals 1 when the sodium ion is in the vicinity of the surfactant head, 0, otherwise. The correlation function is expected to decay from 1 to 0 as time progresses in response to the movement of sodium ions. The slower the decay, the longer the counterions reside near the surfactant headgroups.

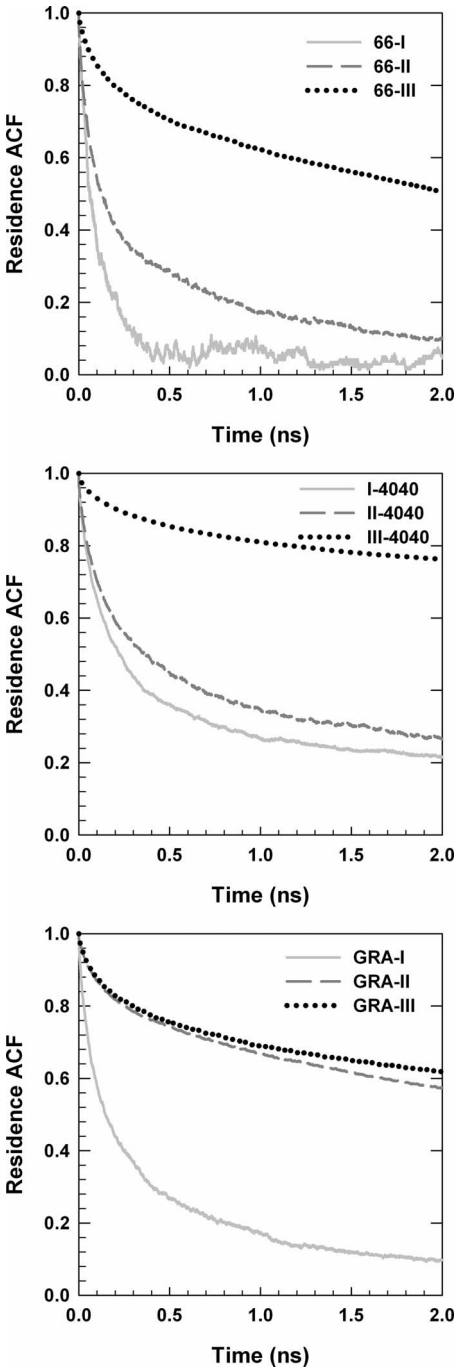

FIG. 6. Residence correlation functions for sodium ions in the vicinity of SDS headgroups. Results are shown for SDS surfactants on (6,6) SWNTs (top), inside (40,40) SWNTs (center), and on graphite (bottom) at three surface coverages. Simulation details are shown in Table I.

In Fig. 6 we show the residence correlation function for the sodium counterions obtained during the different simulations. We observe that at similar surface coverage the sodium counterions stay longer near the SDS headgroups in the case of the I-4040 system compared to systems 66-I and GRA-I.

On (6,6) SWNTs (top panel of Fig. 6), when the surface area per each surfactant is ~ 1.8 nm^2, the correlation function decreases very rapidly. From Fig. 1 we had observed that at this surface coverage, most of the surfactants adsorb on the nanotube and we could not detect aggregation among SDS surfactants. The absence of aggregation allows for the effective screening between counterions and headgroups by water molecules, resulting in the fast decay of residence autocorrelation function. In fact, in all the plots showed in Fig. 6, we observe that the correlation functions decay faster for the simulations with low surfactant concentrations on all substrates. The correlation functions decay significantly more slowly at high SDS surface densities, i.e., upon the formation of surfactant aggregates. This observation further strengthens our previous results according to which counterion condensation is an important phenomenon that contributes to determine the morphology of surfactant aggregates [16]. The system pressure would likely have an influence on the counterion dynamics, but the association between surfactant headgroups and counterions is the dominant phenomenon that dictates the results in Fig. 6, as demonstrated by additional simulations conducted in the *NPT* ensemble ($P=1$ bar) for SDS on (6,6) SWNTs, and others conducted in the *NVT* ensemble for SDS within (40,40) SWNTs in the presence of different amounts of water molecules. These results are described in Appendix B.

Several experiments and simulations [4–6,13,14,16,24] suggest that self-assembled aggregates have different morphologies within confined regions vs on flat surfaces, and a very well-defined structure of surfactants adsorbed on SWNTs has not yet been observed. From the correlation functions just discussed, it appears that large residence times are indicative of the formation of long-lasting aggregates. On the contrary, short residence times indicate very diffuse and possibly disordered surface aggregate structures. This result may lead to the design of experimental tools to discriminate, e.g., the effectiveness of a given surfactant to stabilize aqueous carbon nanotube dispersions.

IV. CONCLUSIONS

Molecular-dynamic simulations of SDS surfactants adsorbed on the outer surface of (6,6) SWNTs, on graphite, and within (40,40) SWNTs have been performed to assess the effect of curvature on the surfactant aggregate morphology. The changes in aggregate morphology were quantified using radial distribution functions and density profiles. The density profiles indicate that the probability of finding counterions close to headgroups increases with the increase in surfactant density but decreases as the substrate curvature increases at equal SDS surface coverage. The results from residence correlation functions indicate that the mobility of counterions and curvature is inversely related. Especially for surfactants within the (40,40) SWNTs, counterions are packed strongly to the surfactant headgroups and reside for long times next to them.

The results presented confirm that counterion-condensation effects are important in determining the morphology of SDS surface aggregates. By promoting or impeding counterion-condensation phenomena, the substrate curvature is strongly reflected on the morphology of the supported surfactant aggregates.

ACKNOWLEDGMENTS

The authors acknowledge financial support from the U.S. DoE under Contract No. FG02-06ER64239 and from the Oklahoma State Regents for Higher Education. Generous allocations of computing time were provided by the OU Supercomputing Center for Education and Research (OSCER) and by the National Energy Research Scientific Computing Center (NERSC) at Lawrence Berkeley National Laboratory. The authors are grateful to B. P. Grady and B. H. Morrow for helpful discussions.

APPENDIX A: SDS ORIENTATION

From Fig. 1, it is clearly visible that the orientation of SDS molecules on (6,6) SWNTs is mostly parallel to the axis of the nanotube, whereas not all SDS molecules inside the (40,40) SWNTs are parallel to the nanotube axis. On graphite, the SDS molecules adsorb preferentially along the α axes. We quantify these observations in Fig. 7, where we show the probability distribution of the angle formed between the CH_3-S vector of SDS molecules and the nanotube axis when SDS molecules are adsorbed on SWNTs. Angles of 0° and 180° indicate that the SDS molecules are parallel to the nanotube axis. An angle of 90° indicates that SDS molecules are perpendicular to the SWNT axis. For SDS on graphite, the angle shown in Fig. 7 is the one formed by the CH_3-S vector of SDS and the α axes of graphite [39]. It is worth remembering that the SWNTs used in the simulations are of the armchair type; thus, the SWNT axis is parallel to α axis of the graphite sheet rolled up to form the nanotube. In the case of graphite (as well as nanotubes), three symmetry α axes are present, each separated by 60°. Thus in Fig. 7 the angles 0°, 60°, 120°, and 180° are all representative of α axes, all equivalent in the case of graphite, but different with respect to the carbon nanotube axis. The angles 30°, 90°, and 150° correspond to β axes.

In the top left panel of Fig. 7, we compare the population distribution of the orientation angle for SDS at low surface densities on the three substrates (systems 66-I, GRA-I, and I-4040). For SDS on graphite, the population distribution peaks at angles that are multiples of 60°. This preferential orientation is observed when the surface area per surfactant headgroup is ~ 1 nm^2, which corresponds to the formation of one complete monolayer.

The SDS surfactants are oriented parallel to the axis of the (6,6) nanotube. SDS surfactants within (40,40) SWNT are oriented parallel to the axis of the nanotube, but the fraction of the SDS molecules that are parallel is slightly less than that observed in the case of (6,6) SWNTs.

In the middle left panel of Fig. 7, we compare the orientation of SDS molecules whose headgroup is at distances less than 0.6 nm for systems 66-II, GRA-II, and II-4040. On (6,6) SWNTs SDS molecules remain parallel to the nanotube axis.

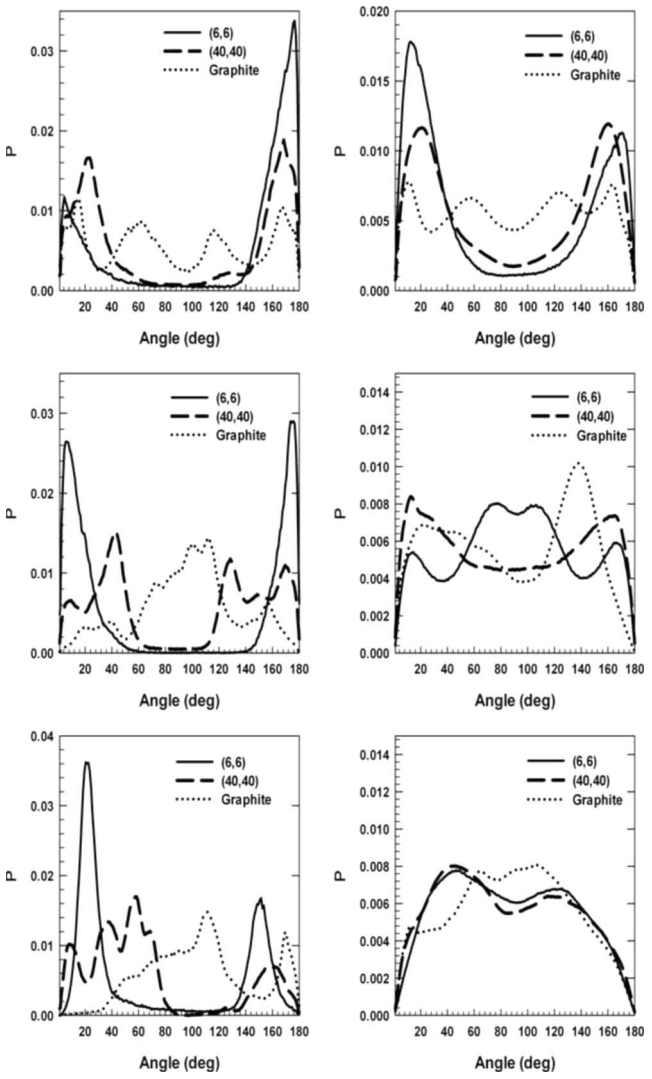

FIG. 7. Left panels: orientation of SDS molecules in the first layer with respect to SWNT axis for (6,6) and (40,40) SWNTs and with respect to the α symmetry axis for graphite. Right panels: SDS-SDS orientation. Top panels report results for systems with low surface density (systems 66-I, GRA-I, I-4040), middle panels are for the results of medium surface densities density (systems 66-II, GRA-II, II-4040), and bottom panels are for the results of high surface densities density (systems 66-III, GRA-III, III-4040). Simulation details can be found in Table I.

On graphite, one broad peak centered at ~100° is observed, indicating that the SDS molecules undergo a reorientation upon increasing the surfactant density.

Within (40,40) SWNTs, the appearance of peaks at 40°, 130°, and 170° indicates that the SDS molecules close to the nanotube surface no longer assume a preferential orientation with respect to the nanotube axis. This happens because for the SDS within (40,40) SWNTs at this surface coverage at least 2 methyl groups in the tailgroup are not adsorbed on the nanotube surface, thus weakening the tail-substrate attractive interactions. This observation agrees qualitatively with previous reports that showed that surfactants or alkyl chains containing less than 12 methyl groups do not orient preferentially when adsorbed on graphite [40–42].

In the bottom left panel of Fig. 7, we show the probability distribution of the first layer of SDS molecules at the largest surface densities considered (systems 66-III, GRA-III, and III-4040). There is a small shift in the intensity of the peak for SDS on 66-III compared to 66-II, i.e., the SDS molecules adsorbed on (6,6) nanotube are oriented at ~20° and 155° with respect to the nanotube axis. In Fig. 3 we had observed that there is a formation of a shapeless surface aggregate on (6,6) SWNTs at high surface density. The features of this aggregate are responsible for the change in surfactant orientation.

On graphite the probability distribution peaks at ~110° and ~170°, indicating that although some surfactants remain oriented along the symmetry axes of graphite, the fraction of molecules oriented along the symmetry axes decreases considerably compared to GRA-I.

Inside (40,40) SWNTs, our results show that there is no particularly preferred orientation for the adsorbed surfactants.

In the right panels of Fig. 7, we show the orientation of SDS molecules with respect to each other. The data are calculated considering all the SDS molecules within each system. This information complements the results provided in the left panels of Fig. 7. For SDS on (6,6) SWNT at low surface coverage (system 66-I), SDS molecules orient either parallel to other SDS molecules or antiparallel to them, as can be evinced from the peaks at ~10° and 170° in the top right panel of Fig. 7.

For SDS on graphite (system GRA-I), we observe regular periodic peaks at multiples of 60°. This information combined with the results for GRA-I from the top left panel of the same figure indicates that the SDS molecules orient along the symmetry axes of graphite.

The results for surfactants inside (40,40) SWNTs (system I-4040) at low surface coverage are similar to those on (6,6)

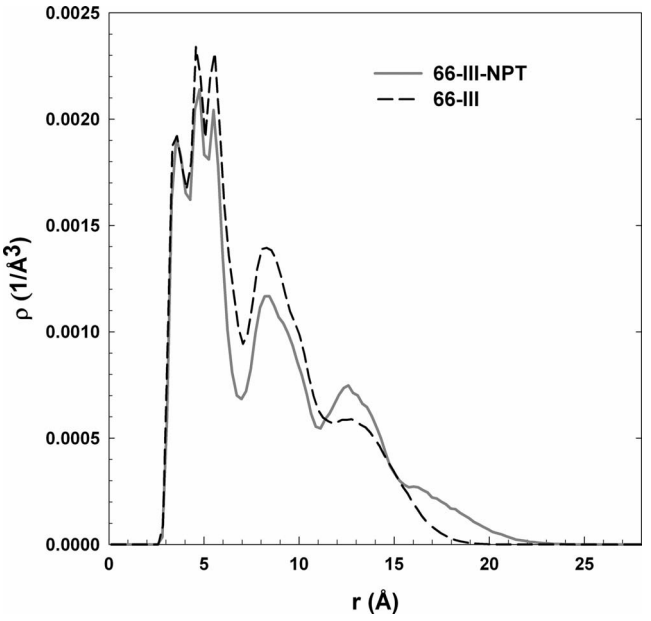

FIG. 8. Headgroup density profiles as a function of distance from the SWNT surface for the system 66-III in the *NVT* (dotted line) and *NPT* (solid line, $P=1$ bar) ensembles.

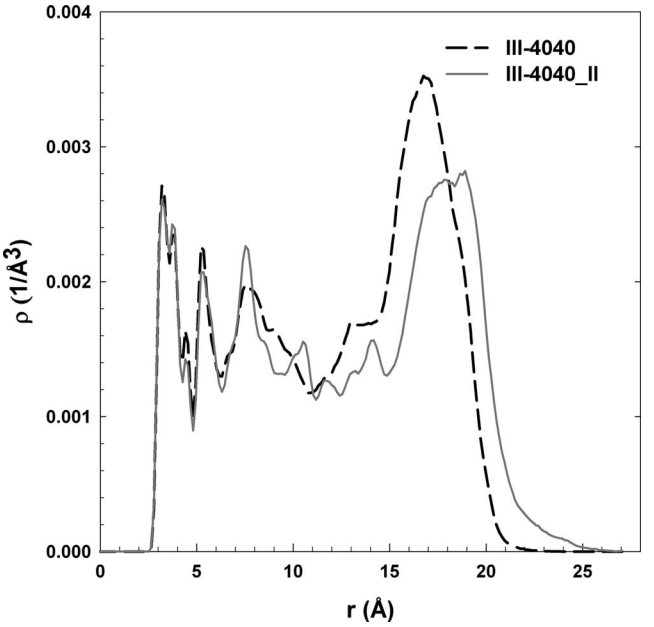

FIG. 9. Headgroup density profiles as a function of distance from the SWNT surface for the system III-4040 (dotted line), with 1680 water molecules, and for the system III-4040_II (solid line), with 668 water molecules.

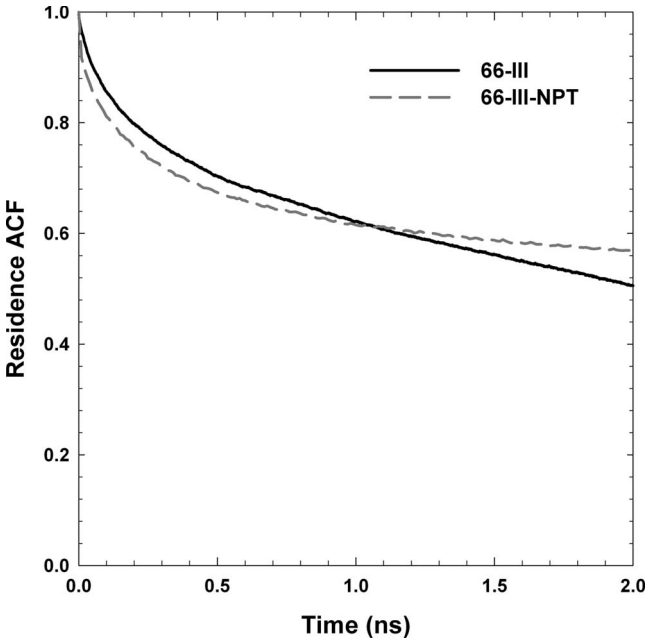

FIG. 10. Residence correlation functions for sodium ions in the vicinity of SDS headgroups. Results are shown for SDS surfactants on (6,6) SWNTs at highest surface coverage in both *NVT* (solid line) and *NPT* ($P=1$ bar, dotted line) ensembles.

SWNTs, i.e., SDS molecules are oriented either parallel or antiparallel to each other.

At medium surface coverage, as shown in the middle right panel of Fig. 7, for surfactants on (6,6) nanotube, the probability distribution of the SDS-SDS angle peaks around 90°. Using the complementary information from the SDS orientation angle presented in the left panels of Fig. 7, we deduce that surfactant molecules that are not within the layer closest to the nanotube are oriented at 90° to each other or at 90° to the molecules present in the layer adjacent to the nanotube. The presence of the first layer allows the subsequent layers to be oriented in any possible angle. For SDS molecules on graphite (system GRA-II), the SDS-SDS orientation peaks at ~140°.

Interestingly, for SDS surfactants within (40,40) SWNT (system II-4040), the probability distribution exhibits two peaks at ~10° and ~170°. At even higher surface densities, the probability distribution of SDS-SDS angle does not have any distinct peaks, as can be observed in the bottom right panel of Fig. 7, indicating that the substrate no longer affects the orientation of the SDS surfactants with respect to each other.

APPENDIX B: PRESSURE EFFECTS

In Fig. 8 we compare the density profiles for the surfactant headgroups on (6,6) SWNTs at the highest surface coverage considered (system 66-III) as obtained running our simulations in either the *NVT* or *NPT* ensembles ($P=1$ bar). Within statistical accuracy, the results are very similar. Namely, the distribution of the headgroups near the surface is almost identical at small distance (up to ~5 Å) from the SWNT surface. The density profiles differ somewhat at larger distances but only with respect to the intensity of the peak, while the peak positions are retained.

In Fig. 9 we compare the SDS surfactant headgroup density profiles within (40,40) SWNTs (system III-4040) with different number of water molecules introduced inside the (40,40) SWNT. The system III-4040-II contains 668 water molecules; the system III-4040 (discussed in the text above) contains 1680 water molecules. Even with this large difference in the number of water molecules inside the (40,40) SWNT, the results are almost identical at small distances from the nanotube surface, but at larger separations (>10 Å) the peaks shift by ~1 Å. These results indicate that the counterion-headgroup association at close distances is insensitive to small changes in pressure in the surrounding fluid. The dynamics of such association, however, may be affected by the pressure, as the pressure directly affects the diffusion and packing characteristics of the particles within and around the surface aggregate.

In Fig. 10 we compare the residence correlation functions for counterions close to the headgroups of SDS surfactants on (6,6) SWNTs at the highest surface coverage in the *NVT* and *NPT* ensembles. The results obtained in the two ensembles are very similar to each other, supporting the conclusion that the results discussed in the present paper are not affected by small changes in the system pressure.

[1] J. N. Israelachvili, *Intermolecular and Surface Forces* (Academic Press, London, 1992).
[2] H. C. Schniepp, D. A. Saville, and I. A. Aksay, J. Am. Chem. Soc. **128**, 12378 (2006).
[3] M. J. O'Connell, S. M. Bachilo, C. B. Huffman, V. C. Moore, M. S. Strano, E. H. Haroz, K. L. Rialon, P. J. Boul, W. H. Noon, C. Kittrell, J. Ma, R. H. Hauge, R. B. Weisman, and R. E. Smalley, Science **297**, 593 (2002).
[4] N. Arai, K. Yasuoka, and X. C. Zeng, J. Am. Chem. Soc. **130**, 7916 (2008).
[5] X. Zhang, D. Cao, and W. Wang, J. Phys. Chem. C **112**, 2943 (2008).
[6] A. K. Jha, J. Lee, A. Tripathi, and A. Bose, Langmuir **24**, 6013 (2008).
[7] C. Gutig, B. P. Grady, and A. Striolo, Langmuir **24**, 13814 (2008).
[8] L. Shi, M. Ghezzi, G. Caminati, P. Lo Nostro, B. P. Grady, and A. Striolo, Langmuir **25**, 5536 (2009).
[9] C. Gutig, B. P. Grady, and A. Striolo, Langmuir **24**, 4806 (2008).
[10] R. Qiao and P. C. Ke, J. Am. Chem. Soc. **128**, 13656 (2006).
[11] Y. Wu, J. S. Hudson, Q. Lu, J. M. Moore, A. S. Mount, A. M. Rao, E. Alexov, and P. C. Ke, J. Phys. Chem. B **110**, 2475 (2006).
[12] C. Richard, F. Balavoine, P. Schultz, T. W. Ebbesen, and C. Mioskowski, Science **300**, 775 (2003).
[13] K. Yurekli, C. A. Mitchell, and R. Krishnamoorti, J. Am. Chem. Soc. **126**, 9902 (2004).
[14] N. R. Tummala and A. Striolo, ACS Nano **3**, 595 (2009).
[15] H. J. C. Berendsen, J. R. Grigera, and T. P. Straatsma, J. Phys. Chem. **91**, 6269 (1987).
[16] N. R. Tummala and A. Striolo, J. Phys. Chem. B **112**, 1987 (2008).
[17] H. J. C. Berendsen, D. van der Spoel, and R. van Drunen, Comput. Phys. Commun. **91**, 43 (1995).
[18] E. Lindahl, B. Hess, and D. van der Spoel, J. Mol. Model. **7**, 306 (2001).
[19] D. van der Spoel, E. Lindahl, B. Hess, G. Groenhof, A. E. Mark, and H. J. C. Berendsen, J. Comput. Chem. **26**, 1701 (2005).
[20] D. Frenkel and B. Smit, *Understanding Molecular Simulations: From Algorithms to Applications* (Academic Press, San Diego, 1996).
[21] U. Essmann, L. Perera, M. L. Berkowitz, T. Darden, H. Lee, and L. G. Pedersen, J. Chem. Phys. **103**, 8577 (1995).
[22] S. Miyamoto and P. A. Kollman, J. Comput. Chem. **13**, 952 (1992).
[23] S. Manne and H. E. Gaub, Science **270**, 1480 (1995).
[24] E. J. Wanless and W. A. Ducker, J. Phys. Chem. **100**, 3207 (1996).
[25] A. B. Jodar-Reyes, J. Lyklema, and F. A. M. Leermakers, Langmuir **24**, 6496 (2008).
[26] Z. Kiraly, G. H. Findenegg, and A. Mastalir, J. Phys. Chem. B **107**, 12492 (2003).
[27] M. Sammalkorpi, A. Z. Panagiotopoulos, and M. Haataja, J. Phys. Chem. B **112**, 2915 (2008).
[28] W. Humphrey, A. Dalke, and K. Schulten, J. Mol. Graphics **14**, 33 (1996).
[29] H. Dominguez, J. Phys. Chem. B **111**, 4054 (2007).
[30] N. R. Tummala and A. Striolo, J. Phys. Chem. B **112**, 10675 (2008).
[31] J. C. Rasaiah, S. Garde, and G. Hummer, Annu. Rev. Phys. Chem. **59**, 713 (2008).
[32] M. J. Rosen, *Surfactants and Interfacial Phenomena* (Wiley-Interscience, Hoboken, New Jersey, 2004).
[33] A. Striolo, A. A. Chialvo, P. T. Cummings, and K. E. Gubbins, J. Chem. Phys. **124**, 074710 (2006).
[34] M. Le Bret and B. H. Zimm, Biopolymers **23**, 287 (1984).
[35] G. S. Manning, Acc. Chem. Res. **12**, 443 (1979).
[36] G. S. Manning, J. Chem. Phys. **51**, 924 (1969).
[37] G. S. Manning, J. Phys. Chem. B **111**, 8554 (2007).
[38] D. Horinek and R. R. Netz, Phys. Rev. Lett. **99**, 226104 (2007).
[39] D. A. Saville, J. Chun, J. L. Li, H. C. Schniepp, R. Car, and I. A. Aksay, Phys. Rev. Lett. **96**, 018301 (2006).
[40] N. B. Holland, M. Ruegsegger, and R. E. Marchant, Langmuir **14**, 2790 (1998).
[41] S. Leggetter and D. J. Tildesley, Mol. Phys. **68**, 519 (1989).
[42] E. Gilbert, P. Reynolds, and J. White, J. Appl. Crystallogr. **33**, 744 (2000).